BIOCHEMISTRY
including biophysical chemistry & molecular biology

Article

pubs.acs.org/biochemistry

# Enzymatic Excision of Uracil Residues in Nucleosomes Depends on the Local DNA Structure and Dynamics

Yu Ye,[†] Mary R. Stahley,[†] Jianqing Xu,[‡] Joshua I. Friedman,[†] Yan Sun,[†] Jeffrey N. McKnight,[§] Jeffrey J. Gray,[‡] Gregory D. Bowman,[§] and James T. Stivers*[,†]

[†]Department of Pharmacology and Molecular Sciences, Johns Hopkins University School of Medicine, WBSB 314, 725 North Wolfe Street, Baltimore, Maryland 21205, United States

[‡]Department of Chemical and Biomolecular Engineering and [§]T. C. Jenkins Department of Biophysics, Johns Hopkins University, 3400 North Charles Street, Baltimore, Maryland 21218, United States

Supporting Information

**ABSTRACT:** The excision of uracil bases from DNA is accomplished by the enzyme uracil DNA glycosylase (UNG). Recognition of uracil bases in free DNA is facilitated by uracil base pair dynamics, but it is not known whether this same mechanistic feature is relevant for detection and excision of uracil residues embedded in nucleosomes. Here we investigate this question using nucleosome core particles (NCPs) generated from *Xenopus laevis* histones and the high-affinity "Widom 601" positioning sequence. The reactivity of uracil residues in NCPs under steady-state multiple-turnover conditions was generally decreased compared to that of free 601 DNA, mostly because of anticipated steric effects of histones. However, some sites in NCPs had equal or even greater reactivity than free DNA, and the observed reactivities were not readily explained by simple steric considerations or by global DNA unwrapping models for nucleosome invasion. In particular, some reactive uracils were found in occluded positions, while some unreactive uracils were found in exposed positions. One feature of many exposed reactive sites is a wide DNA minor groove, which allows penetration of a key active site loop of the enzyme. In single-turnover kinetic measurements, multiphasic reaction kinetics were observed for several uracil sites, where each kinetic transient was independent of the UNG concentration. These kinetic measurements, and supporting structural analyses, support a mechanism in which some uracils are transiently exposed to UNG by local, rate-limiting nucleosome conformational dynamics, followed by rapid trapping of the exposed state by the enzyme. We present structural models and plausible reaction mechanisms for the reaction of UNG at three distinct uracil sites in the NCP.

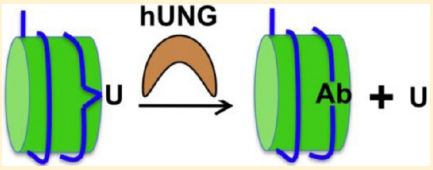


The recognition and repair of damaged DNA bases are largely the tasks of the base excision repair pathway. This pathway is initiated by a variety of DNA glycosylases, each with a different specificity for DNA damage. A common mechanistic problem encountered by these enzymes is the structural obstacle imposed by duplex DNA, which obscures the damaged base within the DNA duplex. Thus, by necessity, these diverse glycosylases have evolved a common strategy for extruding damaged bases from the confines of the DNA duplex and then docking the base in their active sites for catalysis to ensue.[1] This process of "base flipping" requires substantial binding interactions with the DNA backbone, ultimately resulting in substantial DNA bending. An intriguing mechanistic question is how these enzymes operate when a damaged base is embedded in a large protein complex such as a nucleosome, rather than in free duplex DNA.

The enzyme uracil DNA glycosylase (UNG) is the most catalytically robust of DNA glycosylases[2] and shows a remarkable plasticity in locating and excising uracils in duplex or single-stranded DNA contexts and, remarkably, mononucleosomes.[3−6] The enzyme utilizes the favorable opening dynamics of uracil base pairs in free DNA to initiate the process of base flipping,[7,8] suggesting that nucleosome-induced changes in individual base pair dynamics could have a profound effect on the activity of UNG. In this regard, several distinct models can be envisioned to explain the reaction of uracil bases embedded in a nucleosome core particle (NCP) (Figure 1). The simplest model involves direct excision of a uracil without a prerequisite conformational transition in the NCP that exposes the site [$k_{ex}$ for $N_{cl}$ (Figure 1)]. Such a mechanism might hold for sites that are exposed on the surface of the NCP, but steric conflicts between the enzyme and the NCP or reduced base pair dynamics arising from structural aspects of the site could still hinder the reaction compared to that of free DNA. Another model, which has already been established for access of restriction enzymes to their sites,[9,10] is the complete unwrapping of the DNA from the histone octamers [$K^{global}$ (Figure 1)]. With unwrapping as the primary means of UNG accessing nucleosomal DNA, one would expect DNA near the entry or exit sites to react more quickly than internal sites located near the nucleosome dyad axis.[11,12] Indeed, the probability for unwrapping internal sites may be 10000-fold lower than that for end sites,[13] leading to extremely low rates for these sites. A third route for UNG action could involve local

**Received:** May 17, 2012
**Revised:** July 10, 2012
**Published:** July 11, 2012

   dx.doi.org/10.1021/bi3006412 | *Biochemistry* 2012, 51, 6028−6038

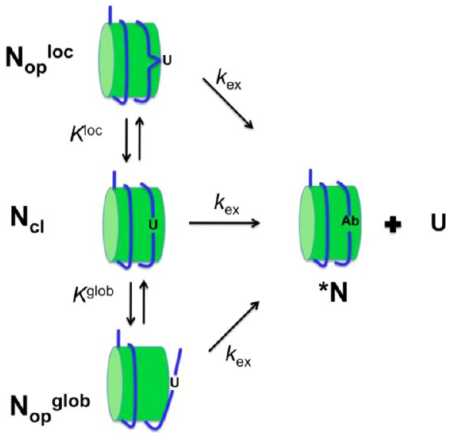


**Figure 1.** Three possible models for uracil excision in the context of a NCP. The NCP is viewed as existing in a closed form where the DNA is wrapped tightly around the nucleosome ($N_{cl}$), and two open forms that differ with respect to whether conformational transitions involving global unwrapping ($N_{op}^{glob}$) or local release ($N_{op}^{loc}$) of the DNA have occurred. In model 1 (middle pathway, $N_{cl}$), a uracil site is exposed even in the context of the closed NCP, and the uracil is excised as rapidly as in free DNA ($k_{ex}$). In model 2 (bottom pathway, $N_{op}^{glob}$), the site is inaccessible to UNG and the lowest-energy pathway to exposing the site is global unwrapping of the DNA from the NCP. This may be described by an unfavorable equilibrium ($K^{glob}$). Once exposed, the site may react with the same excision rate as free DNA. In model 3 (top pathway, $N_{op}^{loc}$), the site is inaccessible to UNG and the lowest-energy pathway to exposing the site is local release of the DNA from the NCP. This may be described by an unfavorable equilibrium ($K^{loc}$). Once exposed, the site may react with the same excision rate as free DNA.

NCP dynamics, rather than global unwrapping [$K^{local}$ (Figure 1)]. The time scale for such dynamics would be determined by local structural features of the site, which could be quite varied for DNA bound to histones. A unique feature of local dynamics is that rapid exposure of sites could occur for sites distant from the DNA ends.

In this report, we have assembled NCPs containing *Xenopus laevis* histones and the 147 bp high-affinity "Widom 601" positioning sequence. Our constructs are identical to a recently published X-ray crystal structure (except for single T/A to U/A substitutions at specific locations)[14] and therefore allow direct interpretation of our kinetic and dynamic measurements using structural parameters. We find that although simple steric considerations and burial of uracils can affect their reactivity with UNG, some uracil sites are reactive even when the crystal structure would indicate a lack of accessibility, and many exposed sites are unreactive. We now propose mechanistic explanations for the reactivities of individual uracil sites in NCPs based on the DNA and histone structural features obtained from the crystal model, as well as small molecule structural probes ($KMnO_4$ and hydroxyl radical) and single-turnover kinetic experiments. In addition, molecular docking of UNG to a highly reactive site in the NCP provides a detailed structural basis for the mechanism of uracil recognition.

## MATERIALS AND METHODS

**DNA Sequences and Nomenclature.** The NCPs were assembled using a minor variant of the 147 bp Widom SELEX 601 DNA sequence employed by Makde et al. in their crystallographic work:[14,15] 601−147b (strand 1), 5′-ATCGGATGTATATATCTGACACGTGCCTGGAGACTAGGGAGTAATCCCCTTGGCGGTTAAAACGCGGGGGACAGCGCGTACGTGCGTTTAAGCGGTGCTAGAGCTGTCTACGACCAATTGAGCGGCCTCGGCACCGGGATTCTCGAT-3′; 601−147b (strand 2), 5′-ATCGAGAATCCCGGTGCCGAGGCCGCTCAATTGGTCGTAGACAGCTCTAGCACCGCTTAAACGCACGTACGCGCTGTCCCCCGCGTTTTAACCGCCAAGGGGATTACTCCCTAGTCTCCAGGCACGTGTCAGATATATACATCCGAT-3′.

The two complementary strands of the Widom 601 sequence (strand 1 and strand 2, given above) are called N1 and N2, respectively, and for the thymine of interest replaced with uracil, the number of nucleotides from the dyad is indicated with a superscript. Following the convention of Richmond and co-workers,[16] the superscript position is either positive or negative, depending on whether the nucleotide of interest is 3′ or 5′ relative to the nucleosome dyad, respectively. Strands 1 and 2 of the Widom 601 sequence correspond to chains j and i, respectively, in the crystal structure of the 601 nucleosome reported by Tan and co-workers [Protein Data Bank (PDB) entry 3MVD].[14] In that structure, the dyad is located at nucleotide 74 on each strand. Therefore, the numbering convention used here can be converted to the nucleotide numbering of the crystal structure by addition of 74. For example, $U^{+22}$N1 corresponds to nucleotide 96 on chain j.

**Preparation of 601 DNA Containing Randomly Incorporated Uracil Residues.** Nucleosomal DNA strands with 147 nucleotides were ordered from Integrated DNA Technologies (IDT) and were purified by polyacrylamide gel electrophoresis using a 6% sequencing gel. Sequenase 2.0 (USB/Affymetrix) was used to randomly incorporate uracil into each strand of DNA at a level of fewer than one uracil per molecule. Polymerase reactions were conducted by using either strand 1 or strand 2 as a template (400 nM) and 400 nM 5′-FAM-labeled 25mer primer complementary to the first 25 bases at the 3′ end of each template. After being heated to 95 °C for 5 min, strands were annealed by being slowly cooled in a buffer consisting of 20 mM Tris-HCl (pH 7.5), 10 mM $MgCl_2$, and 25 mM NaCl. Polymerization reaction mixtures contained 10 μM DTT, standard dNTPs (300 μM each), 30 μM dUTP, and 1 unit of Sequenase/nmol of duplex. Sequencing ladders were constructed using the same conditions except that dUTP was omitted and 30 μM ddATP or ddTTP was added. The reaction was conducted at 37 °C for 45 min, and the extended duplex was isolated using a polymerase chain reaction cleanup kit (Fermentas).

**Formation of Nucleosomes.** Recombinant *X. laevis* histones were expressed individually in bacteria, and the octamer was reconstituted as previously described.[17] NCPs were prepared by adding 400 nM duplex DNA in 2 M NaCl, 10 mM Tris (pH 7.5), 1 mM DTT, and 10 mM EDTA to an equal volume of ~440 nM reconstituted histone octamer in 2 M NaCl, 10 mM Tris (pH 7.5), 1 mM DTT, and 0.25 mM EDTA. The mixture was incubated on ice for 30 min and dialyzed into 10 mM Tris (pH 7.5), 1 mM EDTA, 1 mM DTT, and decreasing amounts of NaCl (1.2, 1.0, and 0.6 M NaCl dialysis steps were performed for 1 h each). The final step of dialysis into a 0 M NaCl solution was performed for 3 h. Complete nucleosomal formation was confirmed using electrophoresis on a native 6% polyacrylamide (60:1 acrylamide:bisacrylamide) gel in 0.25× TBE running buffer, run at 4 °C and 100 V (Figure S1 of the Supporting Information). Only preparations showing a single nucleosome species in which >95% of the input DNA was in the bound form were used for experiments.


dx.doi.org/10.1021/bi3006412 | *Biochemistry* 2012, 51, 6028−6038

**Global Measurements of UNG Activity on Uracilated DNA.** The catalytic domain of human uracil DNA glycosylase (UNG) was expressed in bacteria and purified as previously described.[18] Activity was measured on the randomly uracilated free DNA or in complex with histones under the following conditions: 50 nM nucleosomes (or free 601 DNA), 0.5 nM UNG, 20 mM Hepes (pH 7.5), 10 mM NaCl, 1 mM DTT, 2.5 mM $MgCl_2$, 0.002% Brij 35, and 0.1 mg/mL BSA. Reactions were performed at room temperature and were quenched at various times with 1% SDS. At this time, a 5′-FAM-labeled duplex DNA internal standard was added to each quenched reaction mixture to allow correction for loading differences during gel electrophoresis. For the strand 1 and strand 2 templated experiments, 95 and 72 bp standards were added, respectively. These standards were designed to migrate at positions in the gel where no uracil excision fragments would be found. The reaction mixtures were extracted with equal volumes of a phenol/chloroform/isoamyl alcohol mixture (PCA, 25:24:1, v/v). The aqueous phases were separated and treated with $^1/_{10}$ volume of 1 M NaOH at 95 °C for 10 min. To the resulting solution were added $^1/_{10}$ volume of 3 M NaOAc (pH 5.2), 2.5 μL of 20 mg/mL glycogen, and 3 volumes of cold ethanol. The samples were frozen in −80 °C for 1 h and spun down at 15000*g* for 15 min. The precipitates were dried, dissolved in 5 μL of formamide DNA loading buffer (95% formamide, 0.025% xylene cyanol, and 0.025% bromophenol blue), and loaded on a 6% denaturing polyacrylamide gel. The sequencing gel was run at a constant power of 70 W until the bromophenol blue reached the bottom. The FAM-labeled DNA was detected on the gel with a Typhoon (GE Healthcare) imager with a 520 nm filter and quantified with ImageQuant (GE Healthcare). After normalization to the internal standard on the gel, the fractional reactions of all uracil cleavage bands in the nucleosome and free DNA were calculated using the end point of the free DNA reactions as 100%. The resulting fractional reactions were plotted versus time, and initial rates were determined using linear regression analysis.

**$KMnO_4$ Footprinting.** Freshly prepared nucleosomes (75 fmol) were dissolved in 25 μL of buffer [10 mM Tris-HCl (pH 7.5), 1 mM EDTA, and 1 mM DTT] to a final concentration of 3 nM. The resulting solution was treated with 2 μL of 100 mM $KMnO_4$ (final concentration of 8 mM) for 2 min at room temperature, and then the reaction was quenched with 25 μL of 1.5 M NaOAc (pH 6.2) containing 7% BME. DNA was precipitated using 2 μL of 20 mg/mL glycogen and 150 μL of cold EtOH at 80 °C. The supernatant was carefully removed, and the pellet was dried. Subsequently, 50 μL of 1 M piperidine was added to dissolve the pellet, and the solution was incubated at 90 °C for 30 min, followed by ethanol precipitation as described above. The pellet was then washed with 75% cold ethanol and then precipated again at 80 °C as described above. The supernatant was carefully removed, and the pellet was dried with a gentle air flow. The pellet was dissolved in 7 μL of formamide DNA loading buffer (95% formamide, 0.025% xylene cyanol, and 0.025% bromophenol blue). A 3 μL portion was loaded on a 6% polyacrylamide gel containing 7 M urea, and electrophoresis was performed at 75 W with 1× TBE running buffer until bromophenol blue reached the bottom. The gel was imaged with a Typhoon 8600 (GE Healthcare) imager with a 520 nm filter and quantified with ImageJ (http://rsbweb.nih.gov/ij/).

**Steady-State Kinetic Measurements.** NCPs containing a single uracil at sites $U^{+44}$, $U^{+22}$, and $U^{-32}$ were dissolved in 20 μL of buffer containing 20 mM Tris (pH 7.5), 3 mM EDTA, 1 mM DTT, and 0.002% Brij 35, giving final NCP concentrations of 60, 40, 30, and 15 nM. hUNG was diluted to 0.6 nM in the same buffer, and reactions were initiated by mixing equal volumes of UNG and NCPs. Reactions were quenched with a 2× volume of 0.5 M HCl at various reaction times. Specific reaction times were selected such that less than 30% of the substrate was reacted, and each reaction was performed in triplicate for error estimates. Quenched reaction mixtures were extracted with PCA, and $^1/_{10}$ volume of 10 M piperidine was added, followed by vortexing and centrifugation to separate the aqueous and organic phases. The aqueous layers were heated at 95 °C for 20 min. The resulting solutions were dried in vacuo and resuspended in 150 μL of water followed by the addition of $^1/_{10}$ volume of 3 M NaOAc (pH 5.2), 5 μL of glycogen, and 3 volumes of cold EtOH. The samples were frozen at −80 °C for >1 h and centrifuged for 10 min at 15000*g* and 4 °C. The precipitates were dried, dissolved in 5 μL of 1× formamide load buffer, and loaded on a 6% denaturing polyacrylamide gel. Electrophoreses was performed at 20 W with 1× TBE running buffer until bromophenol blue reached the bottom. The gel was imaged with a Typhoon 8600 (GE Healthcare) imager and quantified with ImageJ. Initial velocities with standard errors were calculated by dividing the amount of product at the time of quench by the elapsed time. Observed steady-state rate constants ($k_{obs}^{ss}$) were obtained by dividing the initial velocities by the UNG concentration. Because saturation could not be achieved with NCP substrates, the second-order rate constant for the steady-state reaction ($k^{ss}$) was obtained from the linear slope of a plot of $k_{obs}^{ss}$ versus substrate concentration using linear regression methods (see the Supporting Information).

**Single-Turnover Kinetic Measurements.** Measurements were performed by manual mixing or by using a Kintek RQ-3 chemical quench-flow instrument depending on the magnitude of the reaction rates. NCPs or free 601 DNA containing a single uracil at sites $U^{+44}$, $U^{+22}$, and $U^{-32}$ was dissolved in a buffer containing 20 mM Tris (pH 7.5), 3 mM EDTA, 1 mM DTT, and 0.002% Brij 35, giving a final concentration of DNA or NCPs of 20 nM. UNG was diluted to final concentrations of 100, 200, or 400 nM in the same buffer. Reactions were performed using pseudo-first-order reaction conditions by mixing equal volumes of hUNG with NCPs (or free 601 DNA). Reactions were quenched with a 2× volume of 0.5 M HCl at various reaction times. The quenched reaction mixtures were extracted with 1:1:1 PCA, and $^1/_{10}$ volume of 10 M piperidine was added, followed by vortexing and centrifugation to separate the aqueous and organic phases. The aqueous layers were heated at 95 °C for 20 min. The resulting solutions were dried in vacuo and resuspended in 150 μL of water followed by the addition of $^1/_{10}$ volume of 3 M NaOAc (pH 5.2), 5 μL of 20 mg/mL glycogen, and 3 volumes of cold EtOH. The samples were frozen at −80 °C for >1 h and centrifuged for 10 min at 15000*g* and 4 °C. The precipitates were dried, dissolved in 5 μL of 1× formamide load buffer, and loaded on a 6% denaturing polyacrylamide gel. Electrophoresis was performed at 20 W with 1× TBE running buffer until the bromophenol blue dye front reached the bottom of the gel. The gel was imaged with a Typhoon 8600 (GE Healthcare) imager, and band volumes were quantified using ImageJ.[19] The fractional extents of reaction were plotted against reaction times and fit to a single-exponential expression, or the sum of two or three exponentials as required. For the DNA substrate $U^{+22}$ and its NCP version $U^{+22}N1$, the single-turnover observed rate


dx.doi.org/10.1021/bi3006412 | *Biochemistry* 2012, 51, 6028−6038

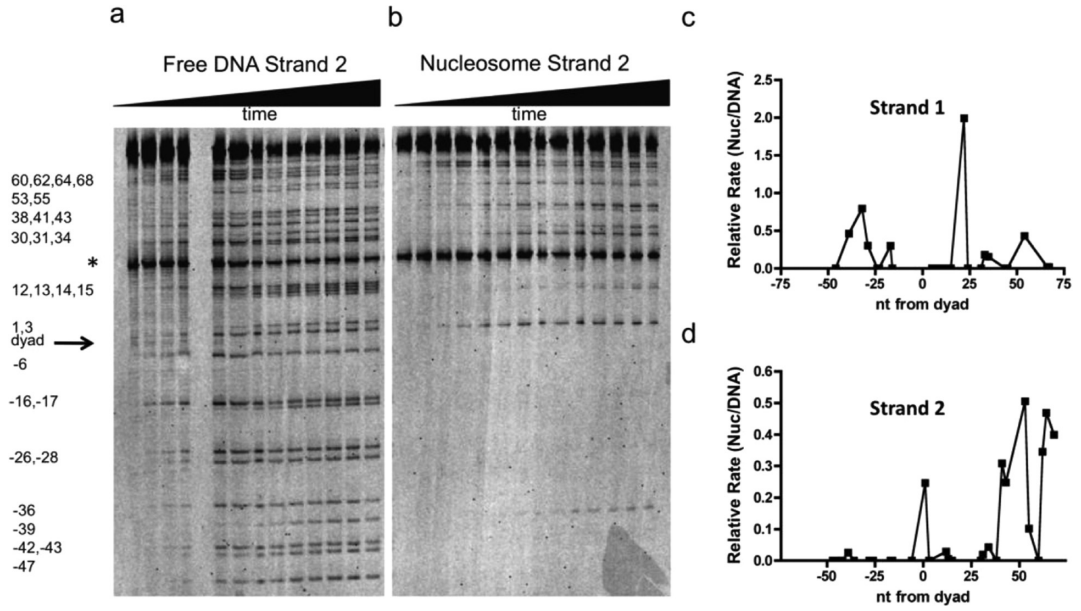


**Figure 2.** Reaction of UNG with free and histone-bound 147 bp 601 DNA containing global T → U substitutions. (a) Denaturing polyacrylamide gel separation of the DNA fragments resulting from base-catalyzed cleavage of the abasic sites generated from UNG excision of uracils. The DNA strand contained a 5′ FAM label and was reacted with hUNG for 0 s, 5 s, 10 s, 20 s, 30 s, 1 min, 2.5 min, 5 min, 10 min, 15 min, 30 min, 60 min, and 95 min (lanes 1−13, respectively, from left to right). The asterisk indicates the migration position of a 5′ FAM-labeled DNA internal standard that was added postreaction to normalize for lane loading differences (see Materials and Methods). (b) Same analysis as in panel a except the DNA is in the context of the NCP. Reaction times are 0 s, 10 s, 32 s, 1 min, 2 min, 5 min, 10.9 min, 20 min, 30 min, 45 min, 60 min, 90 min, 120 min, and 190 min (lanes 1−14, respectively, from left to right). (c and d) Relative activity of UNG for uracil sites in strands 1 and 2 of free and histone-bound 601 DNA. The relative activity is defined as the initial rate of a uracil site in the NCP divided by that of the same site measured in free DNA.

constants ($k_{obs}^{sto}$) were plotted versus the concentration of UNG and fit to eq 1

$$k_{obs}^{sto} = k_{ex}^{sto}/(K_{0.5}/[E_{tot}] + 1) \quad (1)$$

where $k_{ex}^{sto}$ is the maximal uracil excision rate and $K_{0.5}$ is the enzyme concentration that gives the half-maximal rate. The ratio $k_{ex}^{sto}/K_{0.5}$ ($=k'^{sto}$) is the second-order rate constant for single-turnover uracil excision.

**Molecular Docking.** To create a model of enzyme−nucleosome binding at $U^{+22}$N1, the high-resolution part of the RosettaDock protocol was used for all-atom optimization of both backbone rigid-body orientation and side-chain conformation.[20,21] Using the visualization software PyMOL (http://www.pymol.org), the starting structure of docking partners was prepared by superimposing the DNA segment of the UNG−DNA complex (PDB entry 2OXM) onto the nucleosome DNA (PDB entry 3MVD). In the superposition, extrahelical base B5 in the enzyme−DNA complex was aligned to match the position of probed base $U^{+22}$N1 in the nucleosome DNA. On the basis of the UNG−DNA binding mode, base $U^{+22}$N1 must flip out of the DNA helix to allow residue Leu272 in the UNG active site to enter into the minor groove. To satisfy this precondition, the backbone atom coordinates of nucleotides $^{+21}$N1 to $^{+25}$N1 in the nucleosome DNA (PDB entry 3MVD) were replaced by the B4−B8 backbone coordinates in the superimposed DNA segment (PDB entry 2OXM), without changing the original DNA sequence. Using PyRosetta,[22] the high-resolution docking simulations were then conducted with the structure of the superimposed enzyme and the modified nucleosome applying Rosetta's DNA scoring function.[23] No artificial constraint potentials were employed to bias the binding. The simulation generated 20 candidate models. The model with lowest interface energy was selected and is shown in Figure 7.

## RESULTS AND DISCUSSION

There are three substantial advantages of studying the high-affinity 601 DNA sequence as opposed to other lower-affinity histone−DNA binding sequences. (i) The DNA is held in a single register in the NCP, diminishing the contribution of alternative binding modes. (ii) A high-resolution crystal structure of the 601 DNA in complex with *X. laevis* histones has recently been determined (PDB entry 3MVD).[14] (iii) Restriction enzyme reactivities have been mapped along the sequence, providing a valuable point of comparison.[12] We utilize these favorable attributes in the analyses of the UNG reactivity data.

**Global Assessment of UNG Activity at U/A Pairs in Free and Nucleosome-Bound 601 DNA.** Using an appropriate dUTP:TTP ratio, 601 DNA strands containing on average one U/A pair per strand were synthesized by DNA polymerase primer extension, thereby generating a population of DNA molecules in which each thymine was substituted with uracil. Such constructs allow the global assessment of the steady-state initial rates for hUNG reaction at each uracil site along the DNA for both free and nucleosome-bound DNA (Figure 2a,b and Figure S2 of the Supporting Information). Because of the modest flanking sequence preferences of hUNG for free 601 DNA (Figure 2a), different U/A base pairs showed reactivities that differed by as much as 5-fold (Figure S3a of the Supporting Information).[24] Preferred cleavage sequences were AUA, TUA, and CUA, and less reactive sequences were TUC, AUT, and GUC, which is similar to the flanking base trends previously observed with *Escherichia coli* UNG.[25] In contrast to those of free DNA, the cleavage rates in the context of the NCP


dx.doi.org/10.1021/bi3006412 | *Biochemistry* 2012, 51, 6028−6038

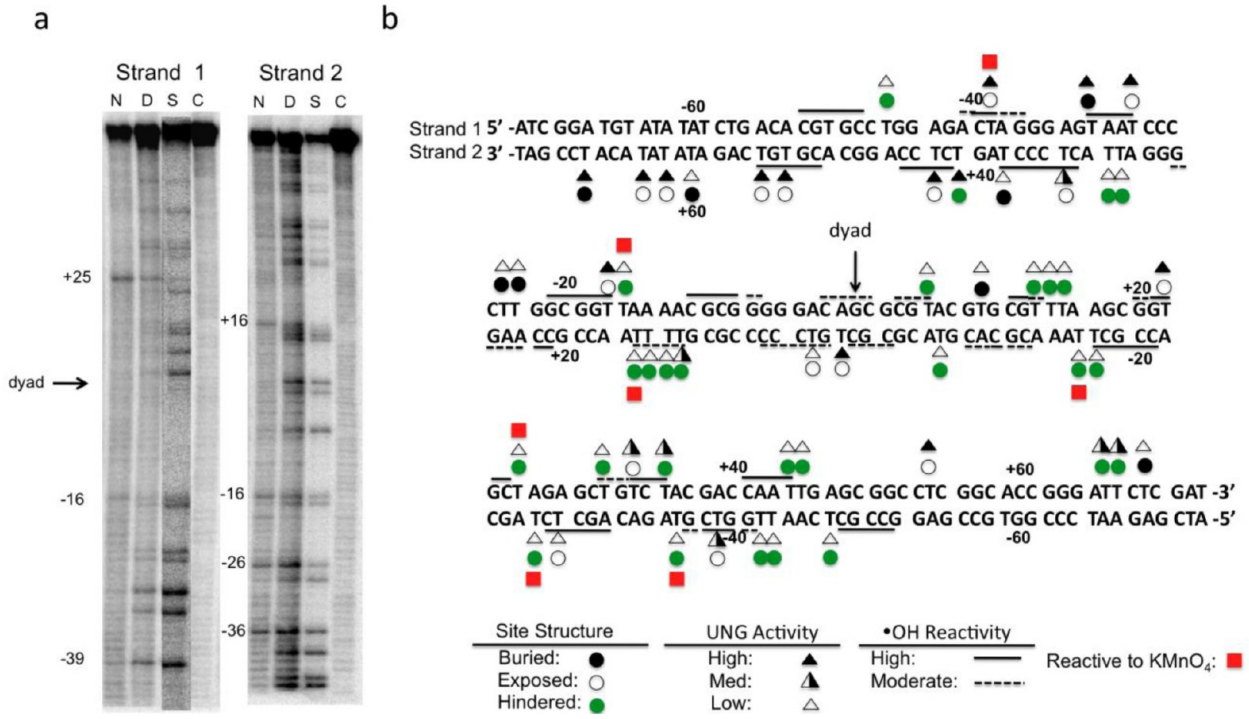


**Figure 3.** Comparison of UNG reactivity with structural properties of the uracil sites in the NCP. (a) $KMnO_4$ footprinting of each strand of the 147mer DNA in the context of the NCP (see Materials and Methods). Abbreviations: N, NCP; D, free DNA; S, single-strand T ladder; C, control (free DNA, no $KMnO_4$). (b) Comparison of the reactivity of hUNG with site exposure in the crystal structure, and $KMnO_4$ and hydroxyl radical footprinting data.[28] Triangles represent the ratio ($R$) between the initial rates for uracil excision in the nucleosome site as compared to the same site in free DNA, with filled, half-filled, and unfilled triangles corresponding to $R$ values of >0.2, 0.02−0.2, and <0.02, respectively. High and moderate sensitivities to hydroxyl radical are indicated by solid and dashed lines, respectively. Red squares indicate high sensitivity to $KMnO_4$ oxidation. Empty, black, and green circles represent rotationally exposed, buried, and rotationally exposed (but otherwise sterically hindered with respect to UNG) uracil sites, respectively.

vary by more than 2 orders of magnitude (Figure 2b and Figure S3b of the Supporting Information), with no obvious sequence trends, suggesting that DNA sequence plays a minor role and that other determinants dominate.

Unlike restriction enzymes, which show a $\sim 10^{-4}$-fold decrease in the efficiency of cleaving their sites as the site is moved from near the DNA entry−exit sites toward the NCP dyad axis,[12] the distribution of UNG-reactive and -unreactive uracil sites across the entire 601 sequence is not clearly related to the position relative to the DNA dyad (Figure 2c,d). Thirty-six of the total of 52 NCP uracil sites showed 0−10% of the activity compared to the same site in free DNA; 14 sites showed 10−60% of the activity, and two sites showed roughly equal and even 2-fold greater activity than free 601 DNA (sites $U^{-32}N1$ and $U^{+22}N1$, respectively) (Figure S4 of the Supporting Information). These reactivity trends, at the very least, indicate that additional mechanisms above and beyond DNA unwrapping must be operative. Thus, local dynamic events or the unique conformations of individual sites must also be important in determining UNG reactivity.

**Correlations between Uracil Site Reactivity and Small Molecule Probes of Duplex Structure.** It is reasonable to expect that UNG-reactive uracil sites might be correlated with their rotational exposure (or lack of steric hindrance) in the crystal structure of the 601 NCP (PDB entry 3MVD). The simplest expectation would be that rotationally exposed uracils (i.e., oriented away from the histone surface as observed in PDB entry 3MVD) would be the most reactive, and buried uracils (oriented against the histone surface) would be the least reactive, as has been previously suggested.[5,6] However, it is also possible that otherwise rotationally exposed residues may also be hindered with respect to the action of UNG because of changes in duplex structural properties or interfering histone side chains.

We looked for possible correlations of the site reactivities with the sensitivity of the 601 DNA sequence to both potassium permanganate, which probes accessibility of the 5,6 double bond of thymidine residues [a surrogate for uracil in the uracilated 601 substrate (Figure 3a)], and hydroxyl radicals, which probe the width of the DNA minor groove.[26,27] Only seven thymidine sites on both DNA strands in the context of NCPs were found to be especially permanganate sensitive (red squares in Figure 3a,b). These sites were also reactive in the free 601 DNA, suggesting that the DNA sequence context of these thymidines plays a substantial role in determining their sensitivity to permanganate in both the free DNA and the NCP. Importantly, all seven of the permanganate sensitive sites were rotationally exposed in the structure, but only one ($U^{-39}N1$) was reactive to UNG. Comparing UNG reactivity results with previously reported NCP hydroxyl radical sensitivity data,[28] we found that only 15 of 26 sensitive sites were also UNG-reactive (Figure 3b, solid and dashed lines). Thus, we find no strong relationship between the reactivity of UNG and small molecule structural probes, even though the reactivity of the small molecules corresponds well with rotational exposure of the site. We conclude that the reactivity of UNG must have higher-order requirements and that these requirements may involve duplex structural properties, the


dx.doi.org/10.1021/bi3006412 | Biochemistry 2012, 51, 6028−6038

presence of interfering histone side chains, or the flexibility of the site in addition to its exposure (see below).

**Correlations between Uracil Reactivity in the NCP and Site Structure.** The expectation that rotational exposure of a uracil site may correlate with its reactivity is largely substantiated because 14 of 20 of the rotationally exposed uracils are moderately or highly reactive, while only 2 of 28 of the buried (or sterically hindered) uracils show similar reactivity (Figure 3). However, we also found that nine uracil sites on strand 1 ($U^{+13,+14,+15}$N1, $U^{+25}$N1, $U^{+31}$N1, $U^{+44,+45}$N1, and $U^{+66,+67}$N1), and five on strand 2 ($U^{6-}$N2, $U^{-16,-17}$N2, $U^{-26}$N2, and $U^{-47}$N2) were unreactive even though they had a rotational position on the nucleosome that appears to expose the site. Closer inspection of these rotationally exposed sites reveals structural features that would likely lead to poor reactivity. The specific features of these sites include one or more of the following: (i) a very narrow minor groove that would impede interactions with an important active site loop of hUNG (see below), (ii) direct hydrogen bonds to the uracil base or phosphate atoms from histone side chains (as inferred from the thymidines in the structure), and (iii) the presence of one or more histone side chains positioned in the minor groove. In addition, site exposure alone fails to explain the absence of reactivity of six highly exposed uracil sites on strand 2 where no obvious structural impediments exist ($U^{+3}$N2, $U^{+12,+13}$N2, $U^{+34}$N2, $U^{-28}$N2, $U^{-39}$N2), nor does it explain the reactivity of two buried sites ($U^{-32}$N1 and $U^{+68}$N2). We conclude that more complicated mechanisms, possibly involving NCP dynamics, must also contribute to the reactivity of these individual sites.

**NCP DNA Structural Parameters and Site Reactivity.** We used the DNA structural analysis program *Curves* and the input file PDB entry 3MVD to investigate whether perturbed 601 base pair structural parameters correlate with the observed uracil reactivities (Figure S5 of the Supporting Information).[29] The first question we explored was whether the subset of exposed sites that were highly reactive had perturbed base pair parameters that might destabilize base stacking and hydrogen bonding interactions at these sites, thereby leading to their enhanced reactivity. For this analysis, a reactive uracil site was defined as an exposed site with >20% of the reactivity of the same site in free DNA. The most highly reactive site in strand 1 ($U^{+22}$N1) showed large perturbations in twist, roll, buckle, tip, and inclination that were among the largest observed across the entire range of NCPs (Figure S5 of the Supporting Information). Thus, these perturbations may increase the dynamic flexibility of this site and lead to its 2-fold greater reaction rate compared to that of the same site in free DNA. The two other exposed sites in strand 1 ($U^{+54}$N1 and $U^{-39}$N1) were ~5 times less reactive than $U^{+22}$N1 and displayed normal B-DNA values for the duplex parameters, except for tip. For the five reactive and exposed sites in strand 2 ($U^{+1}$N2, $U^{+53}$N2, $U^{+55}$N2, $U^{+62}$N2, and $U^{+64}$N2), only one site showed substantial deviations in several duplex parameters ($U^{+1}$N2), and the other sites were not remarkable in this regard. Moreover, we also observed that a number of unreactive exposed sites had perturbed base pair parameters ($U^{+3}$N2, $U^{+34}$N2, $U^{-28}$N2, and $U^{-39}$N2) (Figure S5 of the Supporting Information). We conclude from these analyses that extreme base pair structural parameters can make a given exposed site hyperreactive (i.e., $U^{+22}$N1), but that these considerations alone are in general poorly predictive of the reactivity of exposed sites. One possible explanation for the poor reactivity of some exposed sites is that strong interactions between the histones and DNA at these sites hinder the conformational flexibility required to extrude a uracil base from the duplex. Such energetic effects may arise from interactions some distance from the site and are therefore impossible to discern from inspection of the crystal structure.

One additional feature of several exposed and reactive uracil sites was an exceptionally wide minor groove, and conversely, exposed sites with narrow minor grooves were often unreactive (Figure 4a,b). This is best illustrated in the structural comparison shown in Figure 4c, where the dramatic differences in the minor groove widths for the highly reactive $U^{+22}$N1 (~18 Å) and unreactive $U^{+13}$N1 (~7 Å) sites can be discerned. In terms of the UNG reaction mechanism, a narrow minor groove would place a severe steric impediment to the insertion of the active site loop containing the "wedge" residue Leu272.[18,30−33]

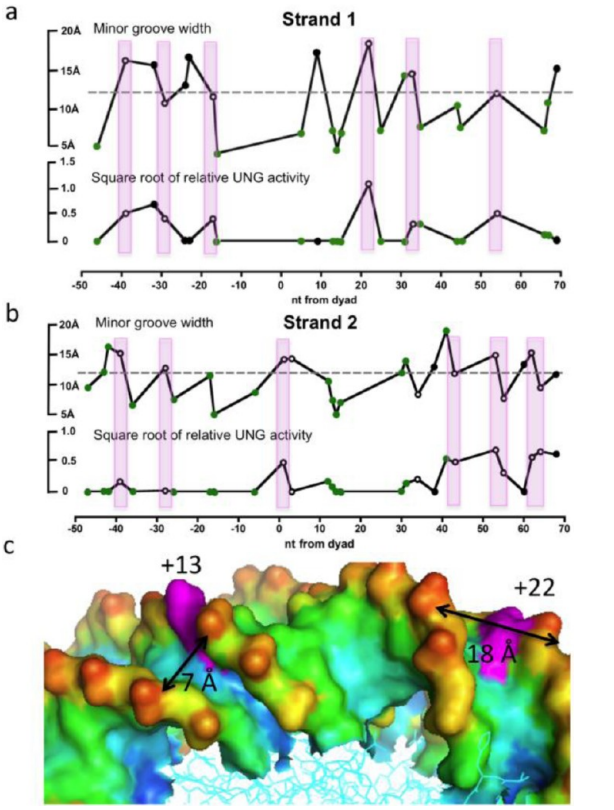


**Figure 4.** Correlations between DNA minor groove width in the NCP and the relative activity of UNG: (a) strand 1 and (b) strand 2. The minor groove widths were obtained by analysis of the X-ray structure using the program *Curves*. The relative UNG activities ($v^{NCP}/v^{free\ DNA}$) are based on our experimental data and are displayed as (relative activity)$^{-1/2}$ to facilitate presentation of small and large values. In these panels, rotationally exposed and buried residues are denoted by empty and filled circles, respectively. The green filled circles denote residues that are rotationally exposed but show other structural features that might inhibit reactivity (histone side-chain interactions or narrow minor grooves). The vertical colored bars indicate those sites that have the following properties: rotational exposure, accessibility to UNG, and average or wider minor groove widths. (c) Structural features of two rotationally exposed residues (magenta) corresponding to $U^{+22}$N1 (reactive) and $U^{+13}$N1 (unreactive), which are located in sites with dramatically different minor groove widths. The other colors in this panel reflect atom depth as calculated using SADIC using a probe radius corresponding to a water molecule (1.4 Å).[46] Red and blue colors denote the most solvent exposed and buried atoms, respectively.


dx.doi.org/10.1021/bi3006412 | *Biochemistry* 2012, 51, 6028−6038

**Table 1. Steady-State and Single-Turnover Kinetic Parameters for Excision of Uracil Sites in Free 601 DNA and in NCPs[a]**

| | $k'^{ss}$ ($\times 10^8$ $M^{-1}$ $s^{-1}$) | $k_{ex}^{sto}$ ($s^{-1}$) | $K_{0.5}$ ($\mu$M) | $k'^{sto}$ [b] ($\times 10^8$ $M^{-1}$ $s^{-1}$) |
|---|---|---|---|---|
| $U^{+44}$ | 1.33 ± 0.03 | 96 ± 13 | 0.76 ± 0.24 | 1.3 ± 0.7 |
| $U^{-32}N1$ | 0.51 ± 0.01 | 10.6 ± 0.2 (36%)[c] | *d* | *d* |
| | | 0.29 ± 0.01 (64%) | | |
| $U^{+22}N1$ | 3.9 ± 0.1 | 166 ± 12 (100%) | 0.45 ± 0.08 | 3.7 ± 0.7 |
| $U^{+44}N1$ | 0.08 ± 0.01 | 24.0 ± 0.1 (23%) | *d* | *d* |
| | | 0.17 ± 0.01 (41%) | | |
| | | 0.003 ± 0.001 (36%) | | |

[a]Errors for the steady-state kinetic measurements were obtained from three replicate experiments performed on two independently prepared nucleosome preparations (two experiments were performed on the first preparation, and the third was performed on the second). The errors shown for the single-turnover kinetic measurements are the standard deviations of the data from the fitted curve for reaction mixtures containing 20 nM NCP and 200 nM UNG. Each time point from the rapid-quench experiment was obtained in duplicate and averaged for plotting. The experiments for $U^{-32}N1$ and $U^{+44}N1$ were repeated at three UNG concentrations (100, 200, and 400 nM) with identical results (Figure 5e,f). These single-turnover data were also collected using two independently prepared nucleosome preparations (the experiments with 100 and 200 nM UNG were performed on one preparation, and the experiment with 400 nM UNG was performed on the second preparation). [b]Obtained from the ratio $k_{ex}^{sto}/K_{0.5}$. [c]Relative amplitude of each kinetic phase. [d]Each kinetic phase was independent of UNG concentration (see Figure 5e,f).

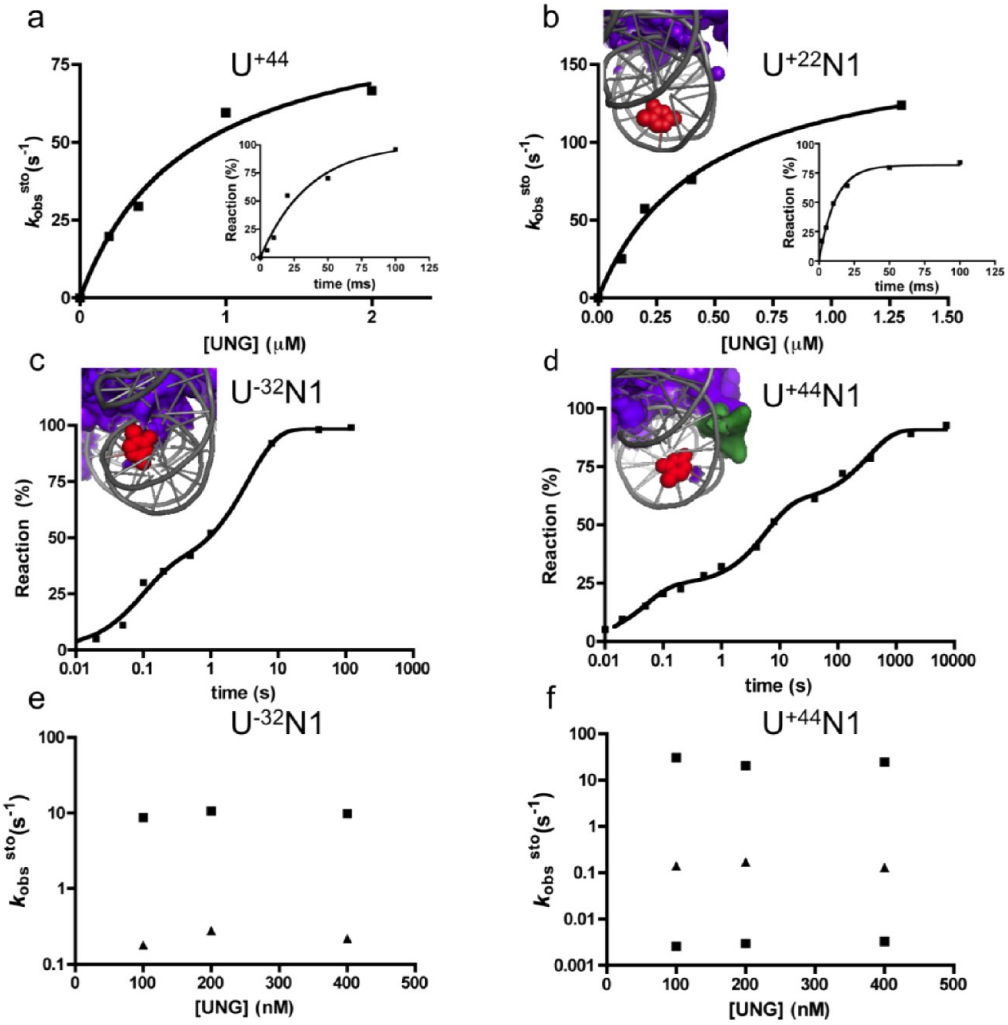


**Figure 5.** Single-turnover kinetic experiments on free DNA ($U^{+44}$) and NCPs containing T → U substitutions at three single sites ($U^{+22}N1$, $U^{-32}N1$, and $U^{+44}N1$). (a) Observed rate constants ($k_{obs}^{sto}$) for the reaction of 20 nM free 601 DNA containing a uracil at site $U^{+44}$ with various concentrations of UNG. The inset shows the kinetic time course with 0.4 $\mu$M UNG. (b) Observed rate constants ($k_{obs}^{sto}$) for the reaction of 20 nM NCP containing a uracil at site $U^{+22}N1$ with various concentrations of UNG. The inset shows the kinetic time course with 1.3 $\mu$M UNG. (c) Time course (log scale) for the reaction of 20 nM NCP containing uracil at site $U^{-32}N1$ with 0.2 $\mu$M UNG. (d) Time course (log scale) for the reaction of 20 nM NCP containing uracil at site $U^{+44}N1$ with 0.2 $\mu$M UNG. In panels b and c, the graphic inserts display the structural properties of each NCP site. The uracils are colored red; the histones are colored purple, and the DNA is colored gray. (e and f) Absence of hUNG concentration dependence for the observed rate constants for single-turnover excision of uracil from nucleosome sites $U^{+44}N1$ and $U^{-32}N1$.


dx.doi.org/10.1021/bi3006412 | *Biochemistry* 2012, 51, 6028−6038

Insertion of this conserved side chain serves to prevent the retrograde motion of the uracil base back into the base stack during the early base flipping step of the reaction.[33,34] It is notable that the most reactive +22 site is located in a region that has been previously suggested to be dynamic. Structurally, this region has been shown to have the capability of "absorbing" one extra base pair or, alternatively, "stretching" if one base pair is deleted.[14] In addition, HIV and intercalating small molecules preferentially insert into this region, which has been attributed to the wide minor groove.[35,36] We surmise that the unusual flexibility or dynamics of this region could very well explain the reactivity of this region to hUNG and to a variety of modifications.

**Steady-State and Single-Turnover Kinetic Reactivities of Individual Uracil Sites Reveal NCP Conformational Transitions.** To further understand the reactivities of uracils embedded in distinct positions of the nucleosome, we turned our attention to three distinct sites with intriguing properties. These sites were investigated individually using both steady-state and single-turnover kinetic methods (Table 1). Site $U^{+22}N1$ is exposed and reacts at a diffusion-controlled rate ($k'^{ss}$) of $4 \times 10^8$ $M^{-1}$ $s^{-1}$ in steady-state measurements of second-order reaction rates (Figure S6 of the Supporting Information). Site $U^{-32}N1$ is buried yet still reacts with a substantial rate ($k'^{ss}$) of $0.5 \times 10^8$ $M^{-1}$ $s^{-1}$ (~40% of the average uracil reactivity in free DNA). Finally, site $U^{+44}N1$ is rotationally exposed but reacts almost 50 times slower than the exposed site $U^{+22}N1$ in steady-state reactions ($k'^{ss} = 8 \times 10^6$ $M^{-1}$ $s^{-1}$). The poor reactivity of $U^{+44}N1$ is likely due to interactions of the flexible N-terminal tail of histone H2A with the minor groove at this site (Ala12, Lys13, Ala14, and Lys15), which is discussed further below.

To further understand the distinct reactivity of these three sites, single-turnover kinetic measurements were performed (Figure 5 and Figure S7 of the Supporting Information). For comparison, we first measured the single-turnover uracil excision rate for a site in free 601 DNA. Such measurements have been previously made for both *E. coli* and human UNG,[37−40] but these measurements were repeated here by placing a single U/A base pair at site $U^{+44}$ in the free 601 DNA (Figure 5a). Similar to previous kinetic findings, the maximal rate of uracil excision at site $U^{+44}$ in free 601 DNA ($k_{ex}^{sto}$) was 96 $s^{-1}$ (22 °C) (Table 1), and the observed second-order rate constant ($k'^{sto}$) was $1.3 \times 10^8$ $M^{-1}$ $s^{-1}$, which was identical to the diffusion-controlled second-order rate ($k'^{ss}$) observed in the steady-state reaction with this same site in free 601 DNA (Figure S6 of the Supporting Information).

The three uracil sites embedded in NCPs showed very different kinetic behavior as compared to that of the free control DNA. Exposed site $U^{+22}N1$ reacted with a single-exponential appearance of product and a hyperbolic dependence on UNG concentration (Figure 5b). The excision rates for $U^{+22}N1$ at each UNG concentration exceeded that of the free DNA by 1.5−2-fold, indicating enhanced second-order ($k'^{sto}$) and maximal excision ($k_{ex}^{sto}$) rates for this site (Table 1). These findings indicate that UNG reacts directly with this site with no requirement for rate-limiting local or global conformational rearrangements of the NCP (see molecular docking studies below). In contrast, buried site $U^{-32}N1$ and exposed site $U^{+44}N1$ both showed multiexponential single-turnover excision rates that were independent of UNG concentration in the range of 100−400 nM (Figure 5c−f). Both sites displayed similar rapid phases (10−20 $s^{-1}$) and a slower phase (0.1−0.2 $s^{-1}$), but site $U^{+44}N1$ also showed a very slow third phase (0.003 $s^{-1}$), necessitating the use of a log time scale to display the data (Figure 5c,d and Table 1). The similar rates for the first two phases with $U^{-32}N1$ and $U^{+44}N1$ suggest that similar conformational processes may be rate-limiting for the reaction of both of these sites even though they are distant from each other in the linear DNA sequence NCP. A common process is a reasonable proposal because these sites are located on adjacent tiers of the DNA chain as it wraps around the histones. The absence of a UNG concentration dependence for excision of $U^{-32}N1$ and $U^{+44}N1$ in the range of 100−400 nM UNG (Figure 5e,f) indicates that rate-limiting conformational changes in the NCP ($k_{conf}$) are required to place these sites in a transient reactive state. Accordingly, UNG must react with these transient states more rapidly than they revert back to an unreactive conformation (i.e., $k_{-conf} < k'^{sto}[UNG]$). A similar mechanism of trapping by UNG is plausible in the human nucleus because UNG is an abundant enzyme (~200000 copies/cell).[2]

**Mechanism of Site Exposure.** At least two related models can be envisioned to explain the multiexponential kinetic reactivity of sites $U^{-32}N1$ and $U^{+44}N1$. First, it is formally possible that these sites exist in multiple stable ground-state conformations, giving rise to different activation barriers for achieving a single UNG-reactive state. In this case, the fractional amplitudes of the individual kinetic phases would represent the populations of the ground-state conformations at the initiation of the reaction. For this simple model to hold, each ground-state conformation should not interconvert during the time frame of the UNG reaction. However, if interconversion of the ground-state conformations does occur (a more plausible scenario), then excision would proceed via a pathway that preferentially funnels through the conformation with the lowest activation barrier for transition to the UNG-reactive state (Figure 6). Despite rapid interconversion, when

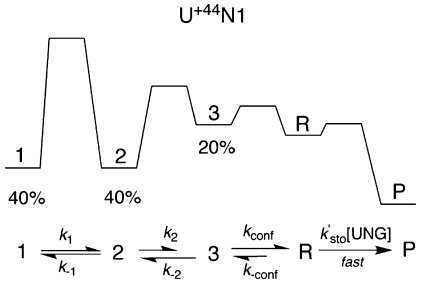


**Figure 6.** Kinetic mechanism for excision of uracil from site $U^{+44}N1$. The single-turnover kinetic measurements for excision of uracil from this site show three kinetic transients (Figure 5d), suggesting that three distinct conformational states of the NCP exist with relative populations of 40% (state 1), 40% (state 2), and 20% (state 3) as depicted in the qualitative free energy reaction coordinate diagram. The rates for conversion of these individual states to the reactive conformation (R) that is competent for uracil excision will depend on the forward rate constants $k_1$, $k_2$, and $k_{conf}$, respectively. In this minimal mechanism, all excision events occur by funneling through the conformation that has the lowest barrier for conversion to the reactive R conformation. The individual rate constants in Table 1 will approximate $k_1$, $k_2$, and $k_{conf}$ under the conditions where (i) $k_1 \ll k_2$ and $k_{conf}$ and (ii) $k_2$ and $k_{conf}$ exceed the corresponding reverse rate constants $k_{-1}$ and $k_{-2}$. The single-turnover kinetic data are independent of UNG concentration, requiring that $k'^{sto}[UNG]$ (for >100 nM UNG) be faster than these NCP conformational changes.


dx.doi.org/10.1021/bi3006412 | *Biochemistry* 2012, 51, 6028−6038

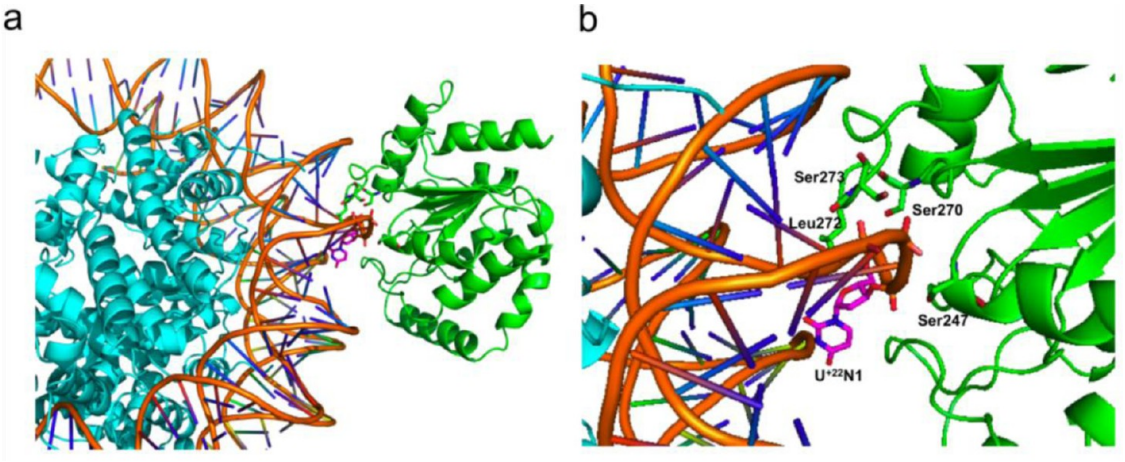


**Figure 7.** Docking-based model for recognition of uracil at the highly reactive site $U^{+22}N1$. (a) View of the docking complex. (b) Expanded view of the docking complex. $U^{+22}N1$, Ser247, Ser247, Ser273, and Leu272 are labeled and shown as sticks.

the reverse rates for the conformational changes are slow compared to the forward steps, this mechanism would also show fractional amplitudes corresponding to different ground-state conformations (see the legend of Figure 6). Although more complicated models are possible, a general mechanism involving a rate-limiting conformational change followed by rapid reaction of UNG is required to satisfactorily account for the excision of uracil from sites $U^{-32}N1$ and $U^{+44}N1$.

Do the observed rates for excision of uracil from sites $U^{-32}N1$ and $U^{+44}N1$ match the conformational transitions previously observed for nucleosomal DNA? Previous studies by the Widom group using ensemble-based stopped-flow fluorescence measurements and FRET fluorescence autocorrelation spectroscopy have led to a model for site exposure that involves successive unwrapping of the DNA duplex from the histone core.[9,41,42] Because the histones tend to contact the DNA about once every turn of the helix, each 10 bp of unwrapping from the DNA entry−exit sites leads to an increased activation barrier largely due to the increasingly unfavorable thermodynamics of breaking multiple histone−DNA interactions. Thus, duplex site exposure rates were around 4 $s^{-1}$ for sites one or two turns from the entry−exit sites, and many orders of magnitude lower for sites three and four turns from the entry−exit sites (~0.02 and 0.002 $s^{-1}$, respectively).[42,43] In contrast, thermodynamically favorable rewrapping rates were rapid and only moderately dependent on position from the entry−exit sites. For instance, the wrapping rate for a site at the dyad axis was 1.4 $s^{-1}$, as compared to 21 $s^{-1}$ for a site one turn from the entry−exit sites.[43] These kinetic values for full duplex unwrapping show little if any agreement with the single-turnover kinetic constants for sites $U^{+22}N1$, $U^{-32}N1$, and $U^{+44}N1$ (Table 1). For site $U^{+22}N1$ (approximately five turns from the nearest edge of the nucleosome), the reaction rate is 6 orders of magnitude greater than the duplex unwrapping rate, and for sites $U^{-32}N1$ and $U^{+44}N1$, located approximately three to four turns from the nearest DNA ends, the rates are ~100−10000 times greater than the expected unwrapping rates. Only the rate of the slowest phase with site $U^{+44}N1$ is in the range expected for duplex unwrapping. These differences are most likely attributed to the DNA binding mode of UNG that does not require full duplex unwrapping. Instead, the reaction of this enzyme is likely to occur directly with some uracil sites (middle pathway, Figure 1) or through local DNA breathing events that are distinct from complete duplex unwrapping (top pathway, Figure 1). These conclusions are supported by the molecular docking studies described below.

**Molecular Docking of UNG to Uracil Sites $U^{+22}N1$, $U^{-32}N1$, and $U^{+44}N1$ in the NCP.** The single-turnover kinetic data described above suggested that UNG could directly dock to uracil site $U^{+22}N1$, but that conformational transitions were required for sites $U^{-32}N1$ and $U^{+44}N1$. We tested these kinetic predictions using a molecular docking approach.[21] To obtain good restraints for the initial docking model, we employed the crystal coordinates of the complex of hUNG with undamaged duplex DNA (PDB entry 2OXM).[31] This is a reasonable model for these purposes because it reflects a very early step along the reaction coordinate where the enzyme has formed nascent interactions with a U:A base pair but has not yet severely bent the DNA duplex as observed in later stage Michaelis complexes.[31,44] Using this model, attempts to dock UNG to sites $U^{-32}N1$ and $U^{+44}N1$ were unsuccessful because of severe steric clashes with the histone core (site $U^{-32}N1$) or with histone N-terminal tail side chains that were present in the DNA minor groove [site $U^{+44}N1$ (see above)] (Figures S8 and S9 of the Supporting Information). These docking attempts clearly indicated the need for conformational transitions for UNG to react with these sites as required from the single-turnover kinetic measurements described above. Although the detailed aspects of these transitions cannot be discerned from these studies, they are likely to involve transient release of the histone tail and/or breaking of local ionic interactions releasing the duplex partially or completely from the histone surface. An additional implication from these findings is that histone tail modifications could have a strong effect on the reactivity of certain sites (i.e., site $U^{+44}N1$).

In contrast with the unreactive sites, it was straightforward to dock UNG on site $U^{+22}N1$ using the same 2OXM model (Figure 7a,b). This docking procedure was restrained using several well-studied interactions of UNG with the DNA phosphate backbone (Ser247, Ser270, and Ser273),[32,45] and the requirement for positioning of the wedge residue Leu272 in the minor groove.[24,43] Using these restraints, converged models were readily obtained with good docking scores. The model provides structural information that helps explain the high reactivity of this site. First, the highly perturbed base pair parameters twist, roll, buckle, tip, and incline (Figure S5 of the Supporting Information) likely promote breathing of the base pair and generate motions that are on the trajectory for


dx.doi.org/10.1021/bi3006412 | *Biochemistry* 2012, 51, 6028−6038

extrusion of the base from the duplex (Figure 7b). Second, the wide minor groove could facilitate entry of the enzyme loop that contains wedge residue Leu272. The unhindered reactivity of this site indicates how the DNA binding mode of UNG, which emphasizes a limited number of strand interactions immediately adjacent to the damage site, is ideally suited for recognition in diverse contexts of duplex DNA, single-stranded DNA, and nucleosomes.

**Conclusions.** These measurements extend our current understanding of damaged base recognition in the context of nucleosomes. Although previous work has established the importance of the rotational orientation of damaged sites on the nucleosome in their reaction with enzymes such as UNG,[3,5,6] our findings provide additional structural and dynamic insights into the reactivity of several sites embedded in NCPs. Our findings establish the importance of local site dynamics, rather than slow global duplex unwrapping, in the recognition of buried or sterically occluded uracil bases and define the time scale of dynamic events at several sites. The data also suggest that the kinetics of damage recognition will be affected by the modification of histone tails (acetylation and methylation) and that the epigenetic status of chromatin may influence DNA base excision repair. Finally, structural models now demonstrate how direct recognition of a damaged base in the context of an NCP can rapidly occur in the absence of any conformational rearrangement of the histones or DNA.

## ■ ASSOCIATED CONTENT

### Supporting Information

Nine supporting figures further describing the kinetic and structural analyses. This material is available free of charge via the Internet at http://pubs.acs.org.

## ■ AUTHOR INFORMATION


### Corresponding Author

*E-mail, jstivers@jhmi.edu. Phone: (410) 502-2758. Fax: (410) 955-3023.



### Funding

This work was supported by National Institutes of Health Grants GM056834 (J.T.S.), GM078221 (J.J.G.), and GM084192 (G.D.B.).


### Notes

The authors declare no competing financial interest.

## ■ REFERENCES


(1) Friedman, J. I., and Stivers, J. T. (2010) Detection of damaged DNA bases by DNA glycosylase enzymes. *Biochemistry 49*, 4957–4967.

(2) Stivers, J. T., and Jiang, Y. L. (2003) A mechanistic perspective on the chemistry of DNA repair glycosylases. *Chem. Rev. 103*, 2729–2759.

(3) Nilsen, H., Lindahl, T., and Verreault, A. (2002) DNA base excision repair of uracil residues in reconstituted nucleosome core particles. *EMBO J. 21*, 5943–5952.

(4) Beard, B. C., Wilson, S. H., and Smerdon, M. J. (2003) Suppressed catalytic activity of base excision repair enzymes on rotationally positioned uracil in nucleosomes. *Proc. Natl. Acad. Sci. U.S.A. 100*, 7465–7470.

(5) Cole, H. A., Tabor-Godwin, J. M., and Hayes, J. J. (2010) Uracil DNA glycosylase activity on nucleosomal DNA depends on rotational orientation of targets. *J. Biol. Chem. 285*, 2876–2885.

(6) Hinz, J. M., Rodriguez, Y., and Smerdon, M. J. (2010) Rotational dynamics of DNA on the nucleosome surface markedly impact accessibility to a DNA repair enzyme. *Proc. Natl. Acad. Sci. U.S.A. 107*, 4646–4651.

(7) Friedman, J. I., Majumdar, A., and Stivers, J. T. (2009) Nontarget DNA binding shapes the dynamic landscape for enzymatic recognition of DNA damage. *Nucleic Acids Res. 37*, 3493–3500.

(8) Parker, J. B., and Stivers, J. T. (2011) Dynamics of uracil and 5-fluorouracil in DNA. *Biochemistry 50*, 612–617.

(9) Li, G., and Widom, J. (2004) Nucleosomes facilitate their own invasion. *Nat. Struct. Mol. Biol. 11*, 763–769.

(10) Li, G., Levitus, M., Bustamante, C., and Widom, J. (2005) Rapid spontaneous accessibility of nucleosomal DNA. *Nat. Struct. Mol. Biol. 12*, 46–53.

(11) Polach, W. J. (1995) Mechanism of protein access to specific DNA sequences in chromatin: A dynamic equilibrium model for gene regulation. *J. Mol. Biol. 254*, 130–149.

(12) Anderson, J. D., Thastrom, A., and Widom, J. (2002) Spontaneous access of proteins to buried nucleosomal DNA target sites occurs via a mechanism that is distinct from nucleosome translocation. *Mol. Cell. Biol. 22*, 7147–7157.

(13) Anderson, J. D., and Widom, J. (2000) Sequence and position-dependence of the equilibrium accessibility of nucleosomal DNA target sites. *J. Mol. Biol. 296*, 979–987.

(14) Makde, R. D., England, J. R., Yennawar, H. P., and Tan, S. (2010) Structure of RCC1 chromatin factor bound to the nucleosome core particle. *Nature 467*, 562–566.

(15) Lowary, P. T., and Widom, J. (1998) New DNA sequence rules for high affinity binding to histone octamer and sequence-directed nucleosome positioning. *J. Mol. Biol. 276*, 19–42.

(16) Davey, C. A., Sargent, D. F., Luger, K., Maeder, A. W., and Richmond, T. J. (2002) Solvent mediated interactions in the structure of the nucleosome core particle at 1.9 Å resolution. *J. Mol. Biol. 319*, 1097–1113.

(17) McKnight, J. N., Jenkins, K. R., Nodelman, I. M., Escobar, T., and Bowman, G. D. (2011) Extranucleosomal DNA binding directs nucleosome sliding by Chd1. *Mol. Cell. Biol. 31*, 4746–4759.

(18) Slupphaug, G., Eftedal, I., Kavli, B., Bharati, S., Helle, N. M., Haug, T., Levine, D. W., and Krokan, H. E. (1995) Properties of a recombinant human uracil-DNA glycosylase from the UNG gene and evidence that UNG encodes the major uracil-DNA glycosylase. *Biochemistry 34*, 128–138.

(19) Abramoff, M. D., Magalhaes, P. J., and Ram, S. J. (2004) Image processing with Image J. *Biophotonics Int. 11*, 36–42.

(20) Gray, J. J., Moughon, S., Wang, C., Schueler-Furman, O., Kuhlman, B., Rohl, C. A., and Baker, D. (2003) Protein-protein docking with simultaneous optimization of rigid-body displacement and side-chain conformations. *J. Mol. Biol. 331*, 281–299.

(21) Chaudhury, S., Berrondo, M., Weitzner, B. D., Muthu, P., Bergman, H., and Gray, J. J. (2011) Benchmarking and analysis of protein docking performance in Rosetta v3.2. *PLoS One 6*, e22477.

(22) Chaudhury, S., Lyskov, S., and Gray, J. J. (2010) PyRosetta: A script-based interface for implementing molecular modeling algorithms using rosetta. *Bioinformatics 26*, 689–691.

(23) Ashworth, J., Havranek, J. J., Duarte, C. M., Sussman, D., Monnat, R. J., Jr., Stoddard, B. L., and Baker, D. (2006) Computational redesign of endonuclease DNA binding and cleavage specificity. *Nature 441*, 656–659.

(24) Slupphaug, G., Mol, C. D., Kavli, B., Arvai, A. S., Krokan, H. E., and Tainer, J. A. (1996) A nucleotide-flipping mechanism from the structure of human uracil-DNA glycosylase bound to DNA. *Nature 384*, 87–92.

(25) Eftedal, I., Guddal, P. H., Slupphaug, G., Volden, G., and Krokan, H. E. (1993) Consensus sequences for good and poor removal of uracil from double stranded DNA by uracil-DNA glycosylase. *Nucleic Acids Res. 21*, 2095–2101.

(26) Tullius, T. D., and Greenbaum, J. A. (2005) Mapping nucleic acid structure by hydroxyl radical cleavage. *Curr. Opin. Chem. Biol. 9*, 127–134.

(27) Bishop, E. P., Rohs, R., Parker, S. C., West, S. M., Liu, P., Mann, R. S., Honig, B., and Tullius, T. D. (2011) A map of minor groove shape and electrostatic potential from hydroxyl radical cleavage patterns of DNA. *ACS Chem. Biol. 6*, 1314–1320.

(28) Fernandez, A. G., and Anderson, J. N. (2007) Nucleosome positioning determinants. *J. Mol. Biol. 371*, 649−668.
(29) Lavery, R., Moakher, M., Maddocks, J. H., Petkeviciute, D., and Zakrzewska, K. (2009) Conformational analysis of nucleic acids revisited: Curves. *Nucleic Acids Res. 37*, 5917−5929.
(30) Mol, C. D., Arvai, A. S., Sanderson, R. J., Slupphaug, G., Kavli, B., Krokan, H. E., Mosbaugh, D. W., and Tainer, J. A. (1995) Crystal structure of human uracil-DNA glycosylase in complex with a protein inhibitor: Protein mimicry of DNA. *Cell 82*, 701−708.
(31) Parker, J. B., Bianchet, M. A., Krosky, D. J., Friedman, J. I., Amzel, L. M., and Stivers, J. T. (2007) Enzymatic capture of an extrahelical thymine in the search for uracil in DNA. *Nature 449*, 433−437.
(32) Jiang, Y. L., and Stivers, J. T. (2002) Mutational analysis of the base-flipping mechanism of uracil DNA glycosylase. *Biochemistry 41*, 11236−11247.
(33) Jiang, Y. L., Kwon, K., and Stivers, J. T. (2001) Turning on uracil-DNA glycosylase using a pyrene nucleotide switch. *J. Biol. Chem. 276*, 42347−42354.
(34) Jiang, Y. L., Stivers, J. T., and Song, F. (2002) Base-flipping mutations of uracil DNA glycosylase: Substrate rescue using a pyrene nucleotide wedge. *Biochemistry 41*, 11248−11254.
(35) Pruss, D., Bushman, F. D., and Wolffe, A. P. (1994) Human immunodeficiency virus integrase directs integration to sites of severe DNA distortion within the nucleosome core. *Proc. Natl. Acad. Sci. U.S.A. 91*, 5913−5917.
(36) Davey, G. E., Wu, B., Dong, Y., Surana, U., and Davey, C. A. (2010) DNA stretching in the nucleosome facilitates alkylation by an intercalating antitumour agent. *Nucleic Acids Res. 38*, 2081−2088.
(37) Stivers, J. T., Pankiewicz, K. W., and Watanabe, K. A. (1999) Kinetic mechanism of damage site recognition and uracil flipping by *Escherichia coli* uracil DNA glycosylase. *Biochemistry 38*, 952−963.
(38) Wong, I., Lundquist, A. J., Bernards, A. S., and Mosbaugh, D. W. (2002) Presteady-state analysis of a single catalytic turnover by *Escherichia coli* uracil-DNA glycosylase reveals a "pinch-pull-push" mechanism. *J. Biol. Chem. 277*, 19424−19432.
(39) Parker, J. B., and Stivers, J. T. (2008) Uracil DNA glycosylase: Revisiting substrate-assisted catalysis by DNA phosphate anions. *Biochemistry 47*, 8614−8622.
(40) Grogan, B. C., Parker, J. B., Guminski, A. F., and Stivers, J. T. (2011) Effect of the thymidylate synthase inhibitors on dUTP and TTP pool levels and the activities of DNA repair glycosylases on uracil and 5-fluorouracil in DNA. *Biochemistry 50*, 618−627.
(41) Tims, H. S., and Widom, J. (2007) Stopped-flow fluorescence resonance energy transfer for analysis of nucleosome dynamics. *Methods 41*, 296−303.
(42) Poirier, M. G., Oh, E., Tims, H. S., and Widom, J. (2009) Dynamics and function of compact nucleosome arrays. *Nat. Struct. Mol. Biol. 16*, 938−944.
(43) Tims, H. S., Gurunathan, K., Levitus, M., and Widom, J. (2011) Dynamics of nucleosome invasion by DNA binding proteins. *J. Mol. Biol. 411*, 430−448.
(44) Parikh, S. S., Walcher, G., Jones, G. D., Slupphaug, G., Krokan, H. E., Blackburn, G. M., and Tainer, J. A. (2000) Uracil-DNA glycosylase-DNA substrate and product structures: Conformational strain promotes catalytic efficiency by coupled stereoelectronic effects. *Proc. Natl. Acad. Sci. U.S.A. 97*, 5083−5088.
(45) Werner, R. M., Jiang, Y. L., Gordley, R. G., Jagadeesh, G. J., Ladner, J. E., Xiao, G., Tordova, M., Gilliland, G. L., and Stivers, J. T. (2000) Stressing-out DNA? The contribution of serine-phosphodiester interactions in catalysis by uracil DNA glycosylase. *Biochemistry 39*, 12585−12594.
(46) Varrazzo, D., Bernini, A., Spiga, O., Ciutti, A., Chiellini, S., Venditti, V., Bracci, L., and Niccolai, N. (2005) Three-dimensional computation of atom depth in complex molecular structures. *Bioinformatics 21*, 2856−2860.